Journal of Ocean Engineering and Marine Energy
https://doi.org/10.1007/s40722-026-00475-4

RESEARCH

Integrating artificial intelligence techniques to enhance the performance of hybrid floating breakwater – wave energy converter analysis

Bayan Hamed[1,2] · Mohamed Elkiki[1] · Sherif Abdellah[3] · Asmaa H. Rabie[4,5] · Reda Diab[6,7]

Received: 24 July 2025 / Accepted: 23 January 2026
© The Author(s) 2026

Abstract
This study presents an integrated experimental and computational analysis of hybrid floating breakwaters and Wave Energy Converters (WECs). Laboratory experiments were carried out at the Hydraulic Laboratory at Port Said University using floating breakwaters with different rear-wall designs. Based on the experimental data, a novel Ensemble Floating Breakwaters Prediction (EFBP) model was created by combining three Artificial Intelligence (AI) techniques: Artificial Neural Networks (ANN), Support Vector Machines (SVM), and Gene Expression Programming (GEP). The ensemble method leverages the complementary strengths of these algorithms by averaging to improve prediction reliability and accuracy. The EFBP model showed exceptional performance (R^2 = 0.9928, MSE = 1.4543 × 10^{-4}), surpassing all individual models. This research establishes the EFBP as a robust predictive tool for optimizing hybrid floating breakwater-WEC systems, aiding the development of sustainable marine energy technologies.

Keywords Floating breakwater · Transmission coefficient · Reflection coefficient · Energy coefficient · Artificial Neural Networks · Support Vector Machines

✉ Bayan Hamed
bayan.hamed@eng.psu.edu.eg

Mohamed Elkiki
m_elkiki@eng.psu.edu.eg

Sherif Abdellah
sherif.elsayed@eng.psu.edu.eg

Asmaa H. Rabie
asmaahamdy@mans.edu.eg

Reda Diab
rr_diab@mans.edu.eg

1 Civil Engineering Department, Faculty of Engineering, Port Said University, Fouad City, Egypt

2 Civil Engineering Department, Higher Institute for Engineering and Technology, Manzala, Egypt

3 Coastal/Harbors Engineering, Civil Engineering Department, Faculty of Engineering, Port Said University, Port said, Egypt

4 Computers Engineering and Control Systems Department, Faculty of Engineering, Mansoura University, Mansoura, Egypt

5 Computer Science Department, Arab East Colleges, Riyadh, Saudi Arabia

Symbols

d	Water depth [m]
L	The incident wavelength [m]
$d1$	The immersed front wall [m]
$d2$	The immersed rear wall [m]
da	The diameter of pneumatic air [m]
A	Swept area of the turbine [m^2]
B	Width of model [m]
T	Wave period [s]
γ_w	Specific weight of water [N/m^3]
V	Velocity [m/s]
P	Internal chamber power amplitude [W]
ρ	Density of water, [kg/m^3]
Ht	Transmitted wave height [m]
Hr	Reflected wave height [m]
Hi	Incident wave height [m]

6 Irrigation and Hydraulics Engineering Department, Faculty of Engineering, Mansoura University, Mansoura, Egypt

7 Faculty of Engineering, Mansoura National University, Mansoura, Egypt

Cr	Reflection coefficient
Ct	Transmission coefficient
Ce	The energy coefficient
RMSE	Root Mean Square Error
MAE	Mean Absolute Error
R^2	Correlation coefficient
MSE	Mean Squared Error

Abbreviations

SGD	Sustainable Development Goals
FBs	Floating Breakwaters
OWC	Oscillating Water Column
WEC	Wave Energy Converter
AI	Artificial Intelligence
ML	Machine Learning
ANN	Artificial Neural Networks
GP	Genetic Programming
SVM	Support Vector Machines
GEP	Gene Expression Programming
PSO	Particle Swarm Optimization
EFBP	Ensemble Floating Breakwater Prediction
WG	Wave Gauge
PG	Pressure Gauge
PTO	Power Take Off
FPV	Final Prediction Value

1 Introduction

Coastal regions worldwide face intensifying threats from climate change and human activities, resulting in shoreline erosion, environmental degradation, and increasing energy demands. This is particularly acute in developing nations. Addressing these interconnected challenges requires innovative, multipurpose coastal infrastructures that combine protective functions with sustainable energy generation. Hybrid floating breakwaters (FBs) integrated with Wave Energy Converters (WECs), particularly Oscillating Water Column (OWC) devices, offer a promising dual-purpose solution by attenuating wave energy and producing clean energy. These systems directly support key United Nations Sustainable Development Goals (SDG 7, 9, 11, 13, 14 & 15) (Fan et al. 2023; Harikrishnan and Sreedharan 2025) and strategic national visions, such as Egypt's Vision 2030, which emphasizes climate adaptation and renewable energy. Furthermore, advances in Machine Learning (ML) and Artificial Intelligence (AI) present transformative opportunities for optimizing the design and performance of these complex systems.

A critical factor in the performance of FB-OWC systems is their geometric configuration. Extensive research has investigated the influence of parameters such as the floating body shape (e.g., horizontal, slope, A-type, U-type, pontoon) and the internal geometry of the OWC's pneumatic chamber on hydrodynamic performance and energy extraction (Kennedy and Marsalek 1969; Harms 1979; Bishop 1982; Zhang et al. 2018; Howe et al. 2020; López et al. 2021; Çelik 2022). Studies have demonstrated that modifications to the chamber's front wall, rear wall, stepped bottom, or underwater lips can significantly enhance performance (Ashlin et al. 2016; Elhanafi et al. 2017). For instance, surging front-wall configurations (Deng et al. 2013), U-shaped chambers (Malara et al. 2017), and floating rear bottom corners (Jalani et al. 2022) have all been demonstrated to improve pneumatic chamber efficiency. Crucially, these findings collectively highlight that the geometry of the floating structure's walls, particularly the rear wall, exerts a dominant influence on the internal air column behavior and, consequently, on the primary conversion efficiency.

However, these approaches are insufficient to predict performance parameters such as wave transmission (*Ct*), reflection (*Cr*), and energy coefficients (*Ce*), particularly for complex hybrid structures with varying rear-wall geometries. These limitations lead researchers to explore Artificial Intelligence (AI) techniques as a more reliable approach. In recent decades, the use of AI techniques to forecast wave hydrodynamic coefficients and to evaluate breakwater-WEC systems has been the subject of numerous studies. Artificial Neural Networks (ANNs), Support Vector Machines (SVMs), Genetic Programming (GP), Gene Expression Programming (GEP) illustrate the progression from straightforward single-method implementations to increasingly sophisticated and integrated frameworks. (Deo et al. 2001; Deo and Jagdale 2003; Castro et al. 2014; Elbisy 2015; Robertson et al. 2017; Oliver et al. 2021). Artificial Neural Networks (ANNs) are widely used with high accuracy for a variety of coastal engineering predictions and designs, including wave–structure interactions, wave transmission, seawall erosion, and seabed changes (Clauss et al. 1992; Jeng et al. 2004; Tseng et al. 2007; Lee et al. 2009; Alshahri and Elbisy 2023; Portillo et al. 2024; Nawaz et al. 2025). Support Vector Machines (SVMs) are noted for their strong generalization capability and resistance to overfitting, making them robust for tasks such as breakwater stability prediction and wave hydrodynamics forecasting (Han et al. 2007; Samui and Dixon 2012; Suykens and Vandewalle 1999; Cogdill and Dardenne 2004; Van Gestel et al. 2004; Kim et al. 2014; Gupta and Karmakar 2023; Alshahri and Elbisy 2023). Gene Expression Programming (GEP) offers a distinct advantage by generating explicit, interpretable mathematical formulas, which have proven valuable in predicting wave setup, breakwater behaviors, and seabed sedimentation (Guven and Gunal 2008;

Hashmi et al. 2011; Azamathulla 2012). Recently, hybrid and ensemble approaches (e.g., PSO-ANN, GA-SVM) have shown promise in improving predictive accuracy for specific structures like low-crested or floating pipe breakwaters.

The predictive capabilities of these individual AI techniques have been well demonstrated in specific coastal engineering applications. For instance, ANNs have been successfully deployed to model wave refraction coefficients (*Cr*) with high robustness (Zanuttigh et al. 2013), forecast nearshore wave power (Castro et al. 2014), and predict key parameters like overtopping discharge and transmission coefficients across diverse structures (Formentin et al. 2017). Similarly, SVMs and hybrid ML approaches have shown superior generalization for tasks such as wave transmission prediction over low-crested structures (Kim et al. 2021) and wave overtopping estimation (Alshahri and Elbisy 2023), often outperforming ANNs in terms of reduced overfitting (Mahjoobi and Mosabbeb 2009). Furthermore, GEP has proven effective in generating accurate, interpretable formulas for wave transmission in floating breakwaters (Patil et al. 2012) and wave setup prediction (Dalinghaus et al. 2022), with models validated across laboratory and field scales (Robertson et al. 2017). However, a critical review reveals three persistent limitations relevant to hybrid FB-OWC systems. First, previous studies have typically focused on predicting a single output parameter (e.g., only *Ct* or only overtopping discharge *q*) for a fixed or relatively simple structure. Second, applications targeting the geometrically complex configuration of hybrid floating breakwaters integrated with OWCs remain limited, with notable exceptions like (Patil et al. 2012) being confined to specific breakwater types. Moreover, while the importance of FB–OWC rear-wall geometry has been well established, there is a scarcity of studies that combine targeted physical experiments on this variable with advanced AI modeling to create robust, validated predictive tools. Third, despite the complementary strengths of ANNs in pattern recognition, SVMs in robust generalization, and GEP in physical interpretability, these methods have not been integrated into a combined ensemble framework capable of simultaneously predicting the multi-faceted performance (*Ct*, *Cr*, and *Ce*) required for holistic FB-OWC design optimization. Table 1 shows the comparison of the presented methods learning.

To address these gaps, this study introduces an Ensemble Floating Breakwater Prediction (EFBP) model, a novel AI framework that integrates three complementary ML methods ANN, SVM, and GEP, to simultaneously predict three critical hydrodynamic coefficients (*Cr, Ct*, and *Ce*) for hybrid FB-OWC systems. The model is trained and validated using original experimental data from wave-flume tests with varying rear-wall geometries, ensuring reliability and practical relevance. By leveraging an ensemble approach, EFBP aims to overcome the limitations of single-model predictions, providing a more accurate and generalizable tool for optimizing the design and performance assessment of multifunctional coastal energy and protection structures.

This study is organized as follows: Sect. 2 describes the experimental setup and data. Section 3 outlines the methodology, while Sect. 4 presents the experimental results. Section 5 presents the results and discussion. Finally, Sect. 6 concludes the main findings and future directions.

2 Description of experimental set-up and data

The experimental studies occurred in the wave flume at the Hydraulic Laboratory, Faculty of Engineering, Port Said University. The wave flume measures 13 m in length, 0.3 m in width, and 0.5 m in height. Wave gauges (WG) and pressure gauges (PG) are necessary instruments for collecting experimental data used in model development and model validation. For wave gauges (WG1-WG4), measured incident, transmitted, and reflected wave heights with a high degree of accuracy. One PG was installed on top of the pneumatic chamber to measure changes in internal air pressure. The WG and PG data were integrated to provide the models with reliable inputs, accurately capturing the hydrodynamic behavior and energy conversion efficiencies of the hybrid floating breakwater, as shown in Fig. 1. The model was positioned at the center of the flume, 7.5 m from the wave maker. Four different configurations were analyzed: (a) Model-A, simple pontoon; (b) Model-B, short slope rear wall; (c) Model-C, vertical back wall then short slope; and (d) Model-D, long slope, as shown in Fig. 2. Every model is characterized by opening the top, representing a simulated Power Take Off (PTO) turbine with a chamber diameter of 11 cm. Key parameters measured the hydrodynamic performance of the breakwater include the incident-wave height (*Hi*), reflected-wave height (*Hr*), and transmitted-wave height (*Ht*). The functional relationships defining the breakwater's performance are formally expressed by Eq. 1:

$$\mathcal{F} = (Hi,\ Hr,\ Ht,\ p,\ B,\ d,\ d1,\ d2,\ L,\ g,\ \gamma w,\ da,\ A,\ V) \tag{1}$$

Key parameters include the model width *B*, internal chamber power amplitude *p,* water depth d, front wall draft *d1*, rear wall draft *d2*, wavelength *L*, gravitational acceleration *g*, the specific weight of water γw, chamber diameter *da*, turbine swept area *A*, and flow velocity *V*. Further, the independent input parameters are expressed in the form of Eq. 2 using Buckingham's-π theorem (Shirlal and Rao 2008). The output coefficients (*Cr*), (*Ct*), and (*Ce*) at a floating breakwater

Table 1 Comparison between presented methods

Technique	Proposed Model	Predictions Type	Advantages	Disadvantages
ANN Patil et al. (2011)	HIMMFPB	Transmission coefficient (Ct)	• Effective Data Compression • Hybrid Learning Algorithm (ANFIS) • Statistical Performance	• Complexity of Implementation • Interpretability Issues • Dependence on Quality of Data
ANN Castro et al. (2014)	SWAN	Energy coefficient (Ce)	• Predictive Power • Reduced Need for Detailed Data • Flexibility in Architecture	• Lack of Established Guidelines • Dependence on Training Data
ANN, SVM Kuntoji et al. (2020)	PSO-ANN, PSO-SVM	Transmission coefficient (Ct)	• Avoidance of Local Minima • Generalization Capability • Sparse Solution Representation	• Complex Implementation • Need for Large Datasets • Need for Precise Adjustment
ANN Zanuttigh et al. (2013)	CLASH	Reflection coefficient (Cr)	• Adaptability to Complex Structures • High Predictive Accuracy • Robust Training Process	• Sensitivity to Input Parameters • Dependence on Quality of Data • Potential Overfitting
ANN Garrido and Medina (2012)	ES	Reflection coefficient (Cr)	• Ability to Capture Nonlinear Relationships • Data-Driven Approach	• Black Box Nature • Complexity in Model Training • Dependence on Quality Data:
ANN Formentin et al. (2017)	CLASH database	Discharge coefficient(q), Transmission coefficient (Ct), and Reflection coefficient (Cr)	• Efficiency in Prediction • Adaptability • Comprehensive Input Parameters	• High Data Requirement • Error Variability • Complexity in Training
Ten ML model types Kim et al. (2021)	LCS	Transmission coefficient (Ct)	• Interpretability • Feature Importance Analysis • Flexibility	• Complexity • Data Dependency • Interpretation Challenges

can be expressed as:

$$Cr,\ Ct,\ \text{and} Ce = \mathcal{F}\,(d/L,\ Hi/L,\ B/L,\ d1/d,\ d1/d2) \tag{2}$$

Where (*d/L*) is the relative depth, *Hi/L* is the wave steepness, *B/L* is the relative width, *d1/d* is the relative front depth, and *d1/d2* is the relative draught.

2.1 Data processing

A total of 360 experimental data points were collected and analyzed from the laboratory tests, including a wide range of wave conditions and model configurations. The raw observations include (Hi), (Hr), and (Ht) wave heights, in addition to pressure and flow velocity data inside the oscillating water column chamber for power calculations.

Equation 3, 5 show hydrodynamics coefficients include (Cr), (Ct), and (Ce), which represent the ratio of energy captured within the chamber to the available incident wave energy. The hybrid floating breakwater is considered to have a higher energy conversion performance when the (Ce) value is higher.

$$Cr = \frac{Hr}{Hi} \tag{3}$$

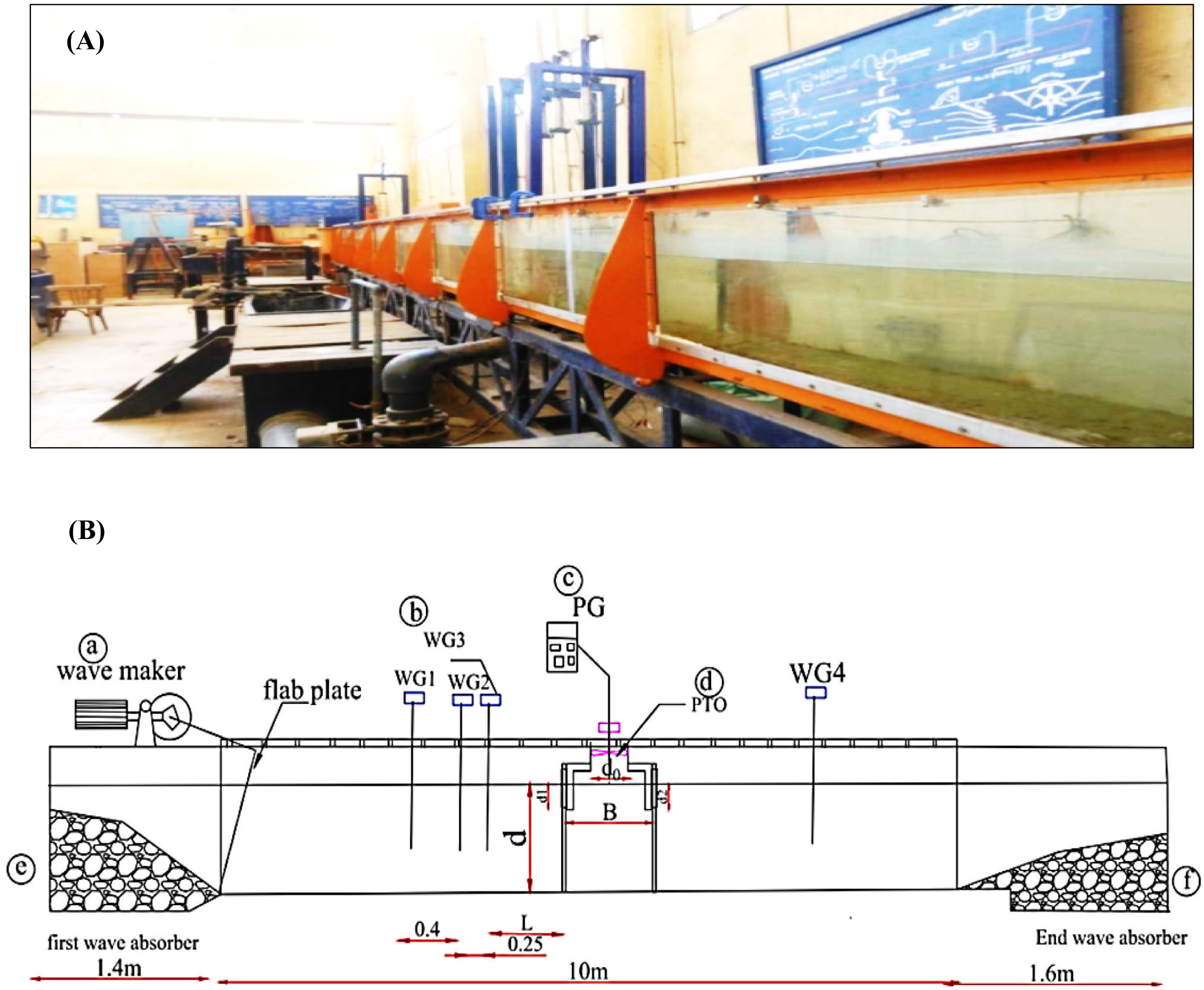

Fig. 1 (**A**) Photos of the WEC-type floating breakwaters system, and (**B**) Schematic view of the experimental setup model position, and wave recording locations: (a) wave maker, (b) WG, (c) PG, (d) PTO, (e) first wave absorber and (f) end wave absorber

$$Ct = \frac{Ht}{Hi} \tag{4}$$

$$Ce = \frac{P}{0.5\rho AV3} \tag{5}$$

where ρ is water density (kg/m^3), $A = \pi r^2$ is the turbine swept area (m^2), and V is the flow velocity (m/s), defined here as $V = L/T$, where L is wavelength (m), and T is wave period.

Each data point was characterized by five non-dimensional input ratios (*d/L, Hi/L, B/L, d1/d*, and *d1/d2*), which describe the relative geometry and hydrodynamic conditions. The calculated coefficients were validated for a selected subset of results by comparison with previous experimental studies before training and testing (Teh and Ismail 2013; Ram et al. 2022; Peng et al. 2024).

3 Methodology

In this section, a hybrid prediction model, the Ensemble Floating Breakwaters Prediction (EFBP) model, is proposed to predict hydrodynamic performance parameters of floating breakwaters, specifically *Cr*, *Ct*, and *Ce*. The model was developed using 360 experimental data points, of which 70% (252 data points) were used for training, and 15% (54 data points) for validation to evaluate the model's performance and generalization capability. According to Fig. 3, the EFBP includes three AI techniques called GEP (Patil et al. 2012), SVM (Balas et al. 2010), and ANN (Mandal et al. 2005). The selection of these models is based on their proven effectiveness and strong overall performance in

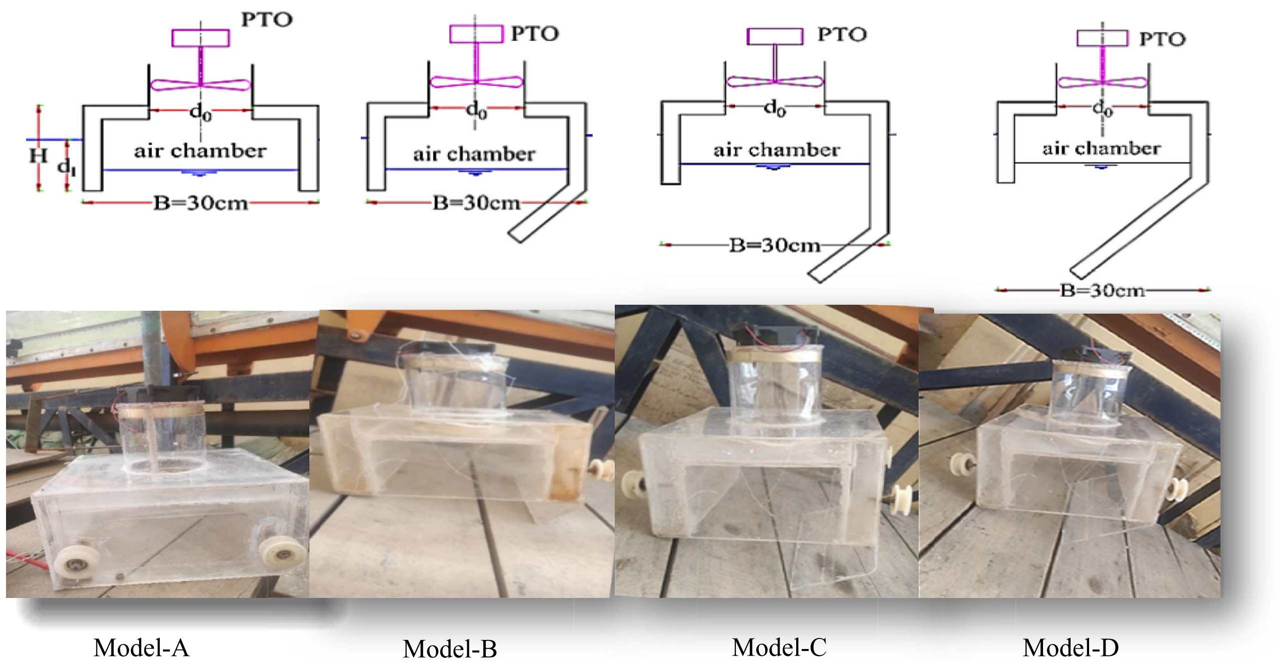

Fig. 2 Details of the tested breakwater models

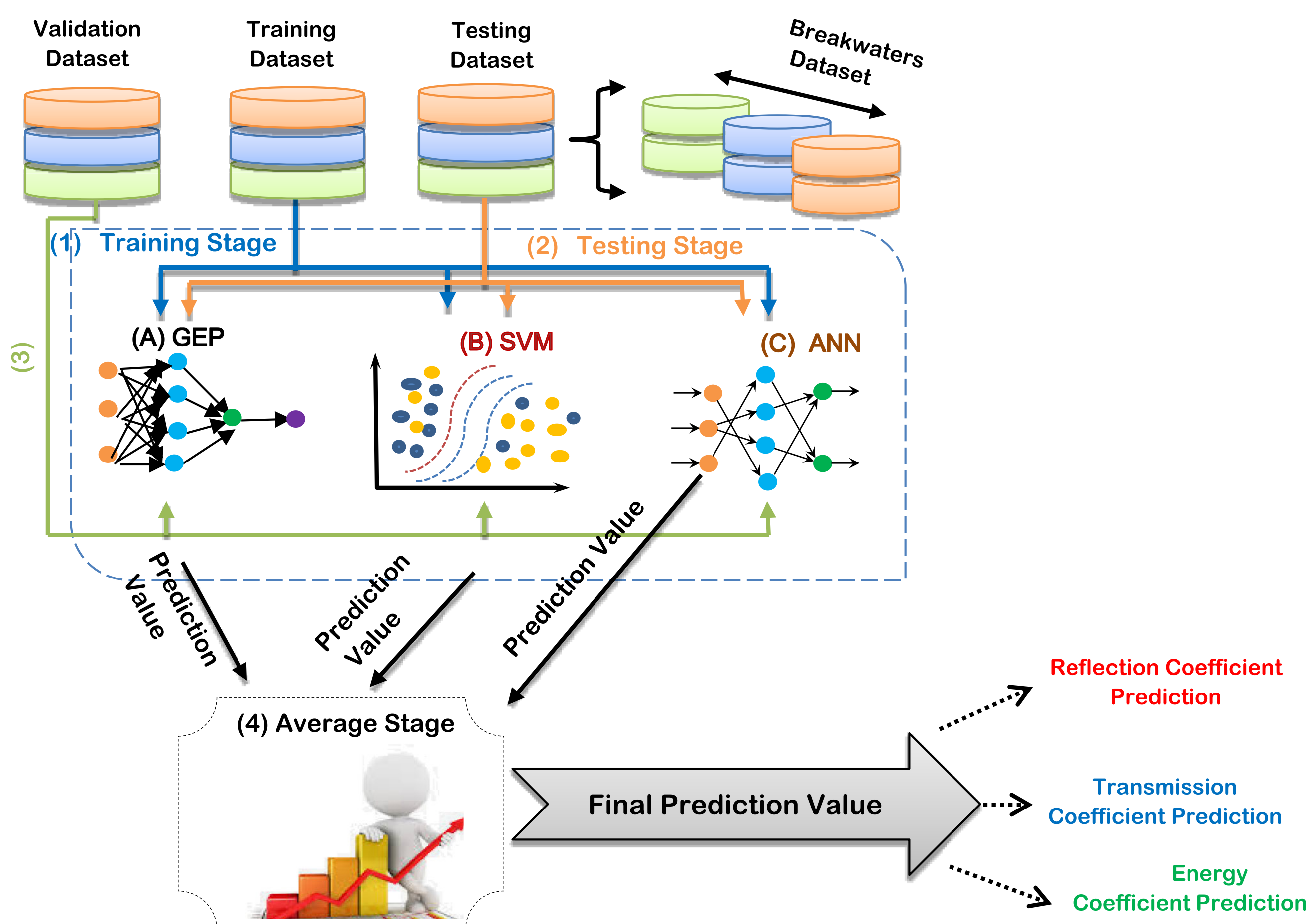

Fig. 3 The steps of Ensemble Floating Breakwater Prediction (EFBP) model

solving regression-based hydrodynamic problems with complex, nonlinear relationships, as consistently demonstrated in coastal and hydraulic research (Abdi Chooplou et al. 2024).

The final prediction is calculated as the arithmetic average of the projections from the three techniques. This fundamental averaging approach combines the outputs of ANN, SVM, and GEP models to achieve complementary strengths and overcome their individual limitations. Specifically, ANN captures nonlinear relationships, SVM significantly improves generalization, and GEP enhances model interpretability. The use of equal-weight was selected because it ensures balanced predictions without introducing bias towards any single model. Furthermore, this strategy effectively avoids the increased complexity and potential overfitting risks associated with more intricate ensemble methods, such as weighted averaging or stacking. The implementation of the EFBP involves four main stages: training, testing, validation, and averaging. During the training stage, the three techniques (GEP, SVM, and ANN) are trained using the training dataset. Next, the models are evaluated on the testing dataset and subsequently validated with the validation dataset.

Finally, the predictions from GEP, SVM, and ANN are combined during this stage to determine the Final Prediction Value (FPV), which is estimated using Eq. 6.

$$FPV(I_i) = \frac{\sum_{k=1}^{c} p_k}{c} \tag{6}$$

where $FPV(I_i)$ is the final prediction value for i^{th} item (I), c is the total number of techniques or prediction values (c = 3), and p_k is the prediction value, where k indicates the number of prediction techniques integrated within the EFBP model.

In this study, the proposed EFBP is applied under three different scenarios, each implemented separately to predict one of the following: (*Cr, Ct, and Ce*).

3.1 Artificial neural network (ANN)

An Artificial Neural Network (ANN) model was used to predict the hydrodynamic coefficients (*Cr, Ct,* and *Ce*) by capturing the complex nonlinear relationships between wave parameters and breakwater geometry, following successful applications in a similar engineering problem (Ghasemi et al. 2016).

The final architecture consisted of three layers: an input layer with five neurons, a single hidden layer with eight neurons using the ReLU activation function, and an output layer with one neuron using a linear activation function, which is effective for regression-based problems (Bungay 2021). For clarity and improved readability, the full weight matrices and bias values are provided in Appendix 1.

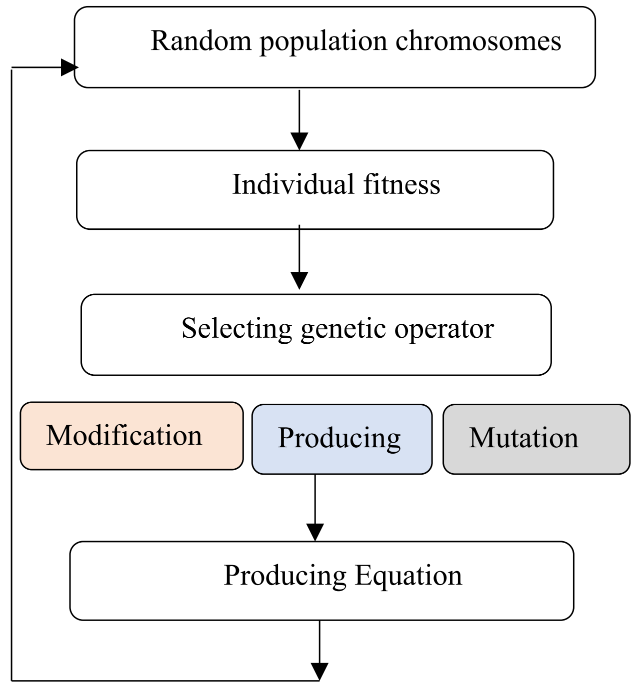

Fig. 4 The steps of the GEP model

3.2 Gene expression programming (GEP)

The GEP approach was introduced by (Ferreira 2010) as a research based on a set of computer programs and is considered an extension of (GP), as described by (Patil et al. 2012). Although each gene has a starting point, its end point may vary and does not correspond to the last position. After this encoding process, the chromosome data decodes into expression trees through a procedure known as translation (Seif et al. 2024). Figure 4 summarizes the main steps of the GEP modeling process.

3.3 Support vector machine (SVM)

The description of the will be presented in this subsection. The SVM is a family of supervised learning methods for regression and classification tasks. These techniques are particularly effective in handling complex non-linear relationships within datasets. The SVM constructs a high-dimensional feature space by transforming the input data, x, using a fixed, non-linear mapping described by (Patil et al. 2012). Within this newly constructed space, a linear model is formulated to find the optimal separating hyperplane, as shown in Fig. 5. A typical approach (converting a linear classifier into a non-linear one) involves mapping the original input space X to a new feature space F of a non-linear function by φ: x → f. Based on the transformed features, the discriminant function is then defined within the F space.

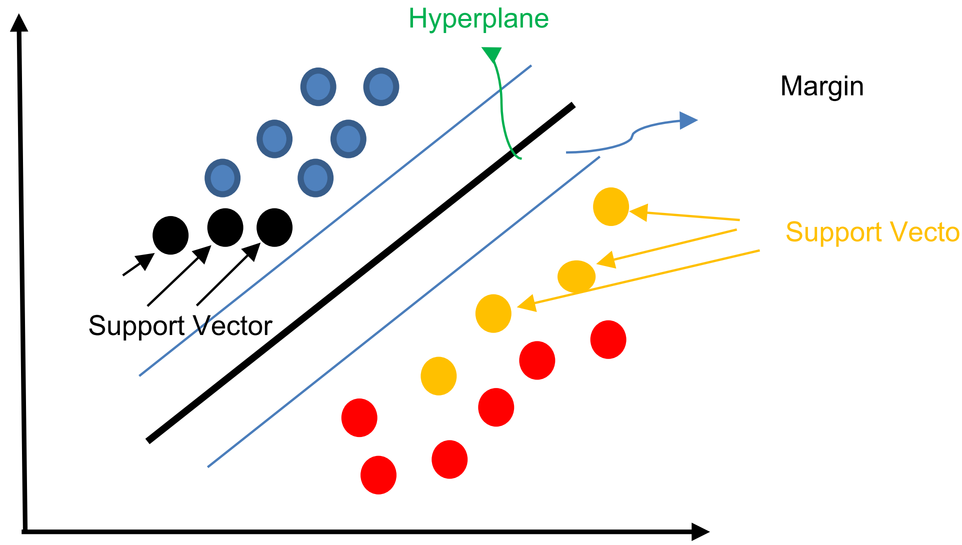

Fig. 5 Architecture of support vector machine

SVM was selected for its robust generalization capability, low susceptibility to overfitting, and proven reliability in modeling small datasets with non-linear behavior. These characteristics make it particularly suitable for predicting the hydrodynamic coefficients examined in this study.

4 Experimental results

The proposed EFBP model, which integrates three AI techniques, ANN, GEP, and SVM, is implemented in the present study. The EFBP model is applied in three different scenarios to predict Cr, Ct, and Ce of the hybrid breakwater. This approach aims to minimize the experimental cost while efficiently evaluating wave attenuation performance.

Four statistical metrics, including the Mean Squared Error (MSE), Correlation Coefficient (R^2), Mean Absolute Error (MAE), and Root Mean Squared Error (RMSE) are used to assess the predictive performance of the applied models. The experimental implementation is carried out through three scenarios corresponding to the output parameters: the first predicts (Cr), the second predicts (Ct), and the third predicts (Ce) based on its data.

4.1 Performance metrics

Four statistical measures called Mean Squared Error (MSE), Mean Absolute Error (MAE), Root Mean Squared Error (RMSE), and Coefficient Determination (R^2) are utilized to evaluate the performance of the proposed EFBP model compared to other models (Eltarabily et al. 2024). Equation 7–10 present the formulations used to compute these metrics:

$$\mathrm{MSE} = \frac{1}{\mathrm{n}}\sum\nolimits_{\mathrm{i}=1}^{\mathrm{n}} (x_i - y_i)^2 \tag{7}$$

$$\mathrm{MAE} = \frac{1}{\mathrm{n}}\sum\nolimits_{\mathrm{i}=1}^{\mathrm{n}} \left|\mathrm{x_i} - \mathrm{y_i}\right| \tag{8}$$

$$RMSE = \sqrt{\frac{\sum (\mathrm{X_{i-Y_i}})^2}{\sum (\mathrm{Xi} - \overline{\mathrm{X}}_\mathrm{i})^2}} \tag{9}$$

$$\mathrm{R}^2 = 1 - \frac{\sum_{\mathrm{i}=1}^{\mathrm{n}} (\mathrm{x_i} - \mathrm{y_i})^2}{\sum_{\mathrm{i}=1}^{\mathrm{n}} (\mathrm{x_i} - \overline{\mathrm{x}}_\mathrm{i})^2} \tag{10}$$

where n is the number of samples in the dataset, xi is the actual parameter coefficient from experimental work, $\overline{\mathrm{x}}\mathrm{i}$ represents the mean of the actual coefficient, and y_i is the predicted coefficient.

5 Results and discussion

This section presents the results of ANN, SVM, GEP, and the proposed EFBP models, in addition to the empirical equations. MSE, MAE, RMSE, and R^2 metrics are used for model evaluation. Each machine learning method (ANN, SVM, GEP, and EFBP) is used for predicting three different hydrodynamic parameters. This comprehensive analysis presents parameters that affect the performance of floating breakwaters.

5.1 Testing EFBP to predict reflection coefficient (*Cr*)

Table 2 presents the descriptive statistics of the collected datasets, focusing on the performance of the four machine learning models. Figure 6a-d compares the actual and predicted values of (Cr) for the ANN, SVM, GEP, and EFBP models. The ANN exhibited the strongest correlation, with

Table 2 Descriptive statistics of the collected datasets (Cr)

Model	MSE	MAE	RMSE	R^2
ANN	$9.070*e^{-7}$	0.043532	0.28476	0.991121
GEP	$6.869*e^{-6}$	$4.807*e^{-4}$	0.18134	0.93032
SVM	0.000277	0.01195	0.186661	0.95
EFBP	$1.454*e^{-4}$	0.07654	0.19877	0.9889

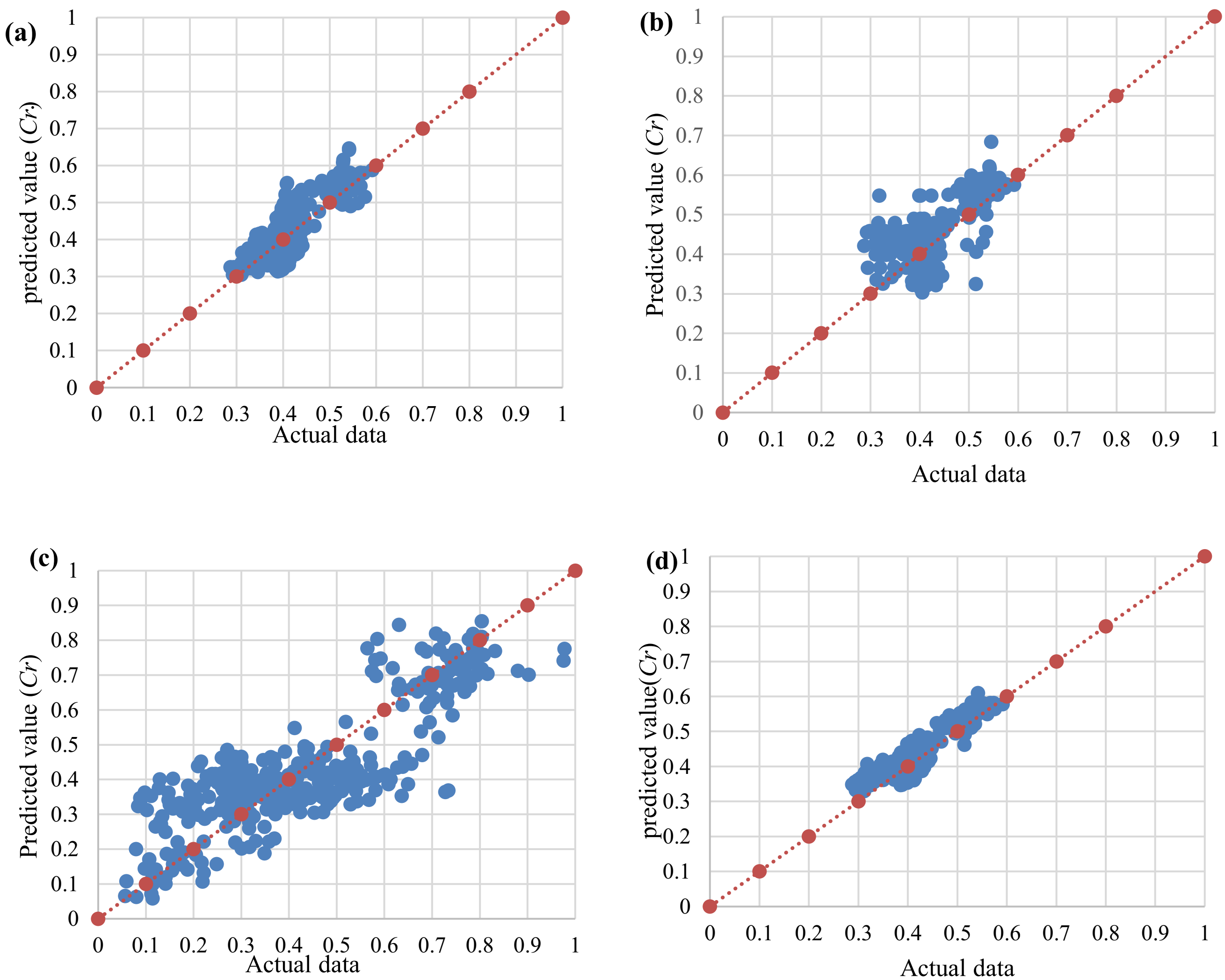

Fig. 6 Shows the comparison between the actual and predicted Cr values using (**a**) ANN (**b**) GEP (**c**) SVM (**d**) EFBP models

predicted values closely aligned along the 1:1 line, indicating high accuracy and strong generalization capacity (Loukili et al. 2025).

In contrast, the SVM and GEP models demonstrated the weakest performance, showing significant deviations from the ideal line, which suggests poor generalization and limited ability to capture the nonlinear behavior of (*Cr*). The proposed EFPB model outperforms all others, with predicted values tightly clustered around the 1:1 line, providing the most consistent and reliable prediction, followed by ANN.

Figure 7a-b compares the model's performance in predicting the (*Cr*) using line and scatter plot representations. In Fig. 7a, the normalized observed (*Cr*) values are compared, and the line graph of the predicted values is shown.

Both ANN and EFBP show strong alignment with the observed value, indicating high predictive accuracy, whereas GEP and SVM exhibit larger deviations. In Fig. 7b**,** the scatter plots of actual versus predicted (*Cr*) values indicate that most points from ANN and EFBP fall within the ± 25% error margin of the perfect agreement line, suggesting accurate and

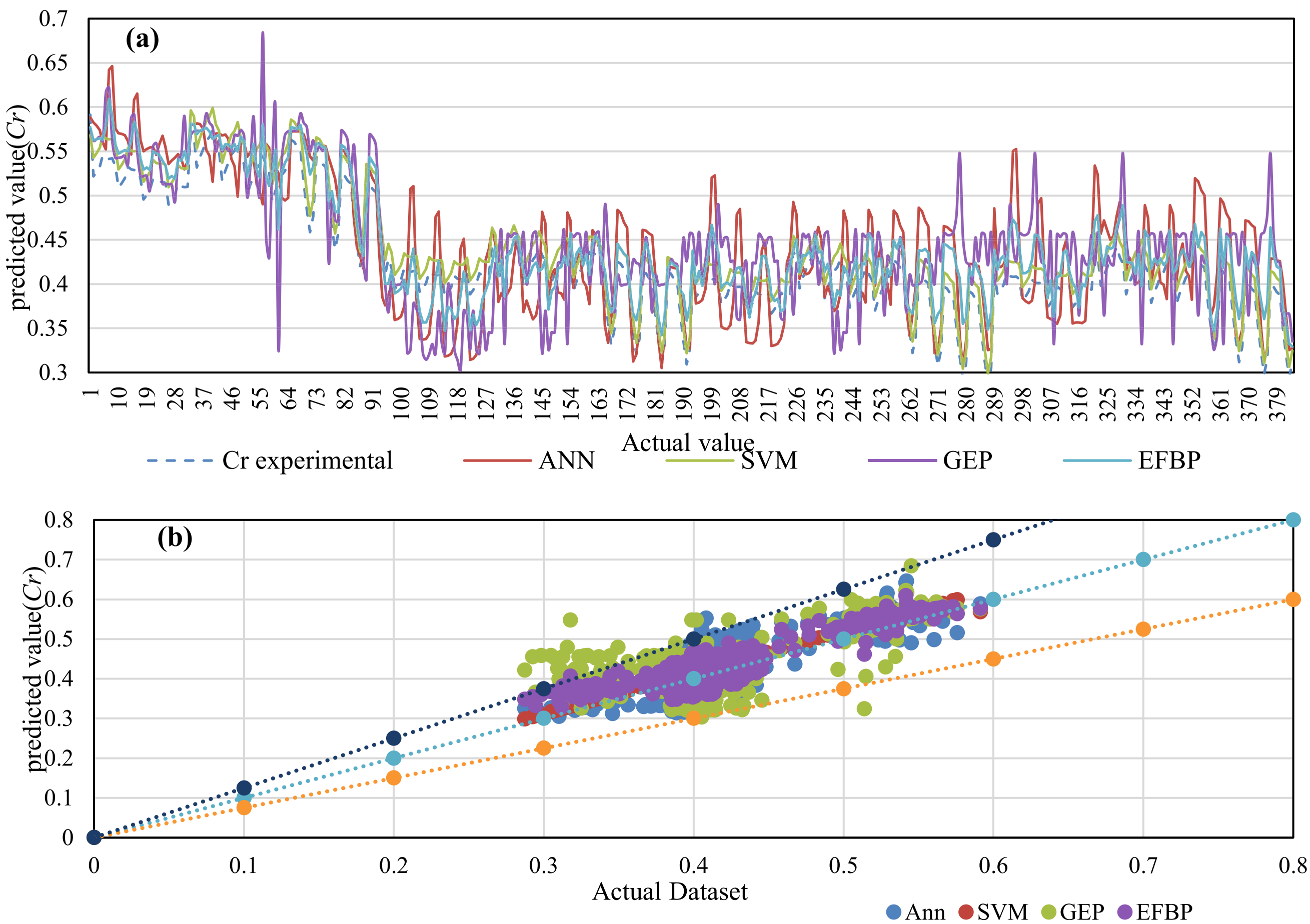

Fig. 7 The representation of actual Cr values vs. predicted values from ANN, SVM, GEP, and EFBP; (**a**) Line graphs representation and (**b**) scatter plots representation

consistent predictions. Conversely, GEP and SVM show a scatter, reflecting lower performance. Overall, the EFBP and ANN outperformed GEP and SVM, with EFBP demonstrating the most consistent and reliable prediction capability.

5.2 Testing EFBP to Predict Transmission Coefficient (*Ct*)

Table 3 presents the statistical performance metrics of four machine learning models, ANN, GEP, SVM, and EFBP, for predicting *Ct*. Figure 8a-d shows the scatter plots of predicted versus actual (*Ct*) values for each model.

As shown in Fig. 8a, the ANN model demonstrates strong predictive performance. The data points closely follow the 1:1 trend line, indicating accurate prediction and consistent alignment with the observed growth pattern. This suggests that the ANN model effectively validates the experimental data and presents reliable predictions, with minor deviations that do not significantly affect overall accuracy (Karami and Saghi 2024).

In contrast, the GEP model in Fig. 8b, shows a scattered distribution of points around the trend line, reflecting lower predictive accuracy and greater deviation from observed values. Conversely, the SVM model in Fig. 8c shows moderate accuracy, with prediction generally following the trend line, although some larger deviations are evident. The EFBP in Fig. 8d model demonstrates a strong clustering of points around the trend line, confirming strong predictive capability, although a slightly wider spread is observed compared to ANN. Overall, the ANN, SVM, and EFBP models outperform the GEP model in predictive accuracy.

In the line graph Fig. 9a, the predicted line from all models generally follows the measured (*Ct*) pattern, though differences in accuracy are apparent, particularly at peak and trough points. The ANN model effectively captures these sharp changes, with the predictions nearly overlapping the observed value. Both SVM and EFBP respond well to dynamic variation but do not reach the same level of accuracy as ANN in some critical regions. Conversely, the GEP model shows limited ability to track abrupt fluctuations, as

Table 3 Descriptive statistics of the collected datasets (Ct).

Model	MSE	MAE	RMSE	R^2
ANN	0.015738	0.043532	0.28476	0.92378
GEP	0.03479	0.1107729	0.18134	0.80
SVM	0.0099368	0.063778	0.0968	0.85
EFBP	0.00123	0.0345	0.296	0.9752

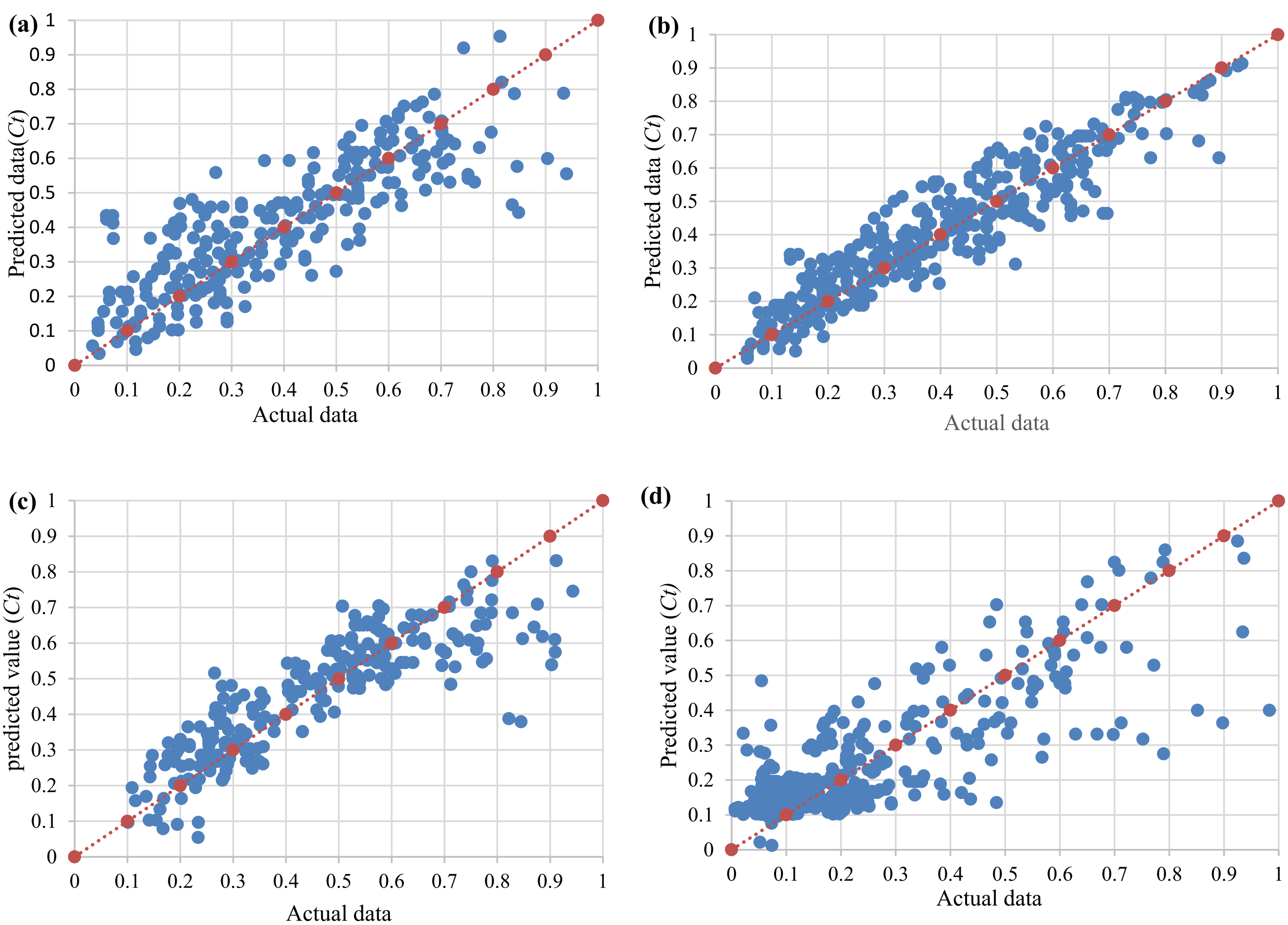

Fig. 8 Shows the comparison between the actual and predicted Ct values using (**a**) ANN (**b**) GEP (**c**) SVM (**d**) EFBP models

its predicted lines deviate more from the observed data, indicating weaker adaptability to nonlinear variations.

In the scatter plot Fig. 9b, points closer to the 1:1 dashed line indicate higher prediction accuracy. The closer the points are to the trend line, the more accurate the model. The ANN model demonstrates tightly clustered points near the line, confirming high predictive reliability. EFBP and SVM also perform well, although their point distribution are slightly wider. The GEP shows a wide spread of points along the lines, and these models are not very accurate in making valuable predictions. Finally, the EFBP model achieved the best overall performance in predicting (*Ct*), followed by ANN and SVM models, while GEP exhibits the weakest accuracy among the models.

5.3 Testing EFBP to predict energy coefficient (*Ce*)

This section compares the performance of the proposed EFBP model in predicting (*Ce*) against three conventional machine learning models: ANN, SVM, and GEP. The evaluation was conducted using four statistical metrics: MSE, MAE, RMSE, and R^2, as presented in Table 4.

As illustrated in Fig. 10a-d, all models demonstrate strong predictive capabilities. Among them, the ANN achieves the highest performance, with $R^2 = 0.93$ and the lowest error metrics (MSE = 0.01456, MAE = 0.072985, RMSE = 0.1218476), indicating excellent prediction accuracy. The EFBP model achieved $R^2 = 0.95$, with slightly higher MSE, MAE, and RMSE than the ANN model, resulting in a slightly

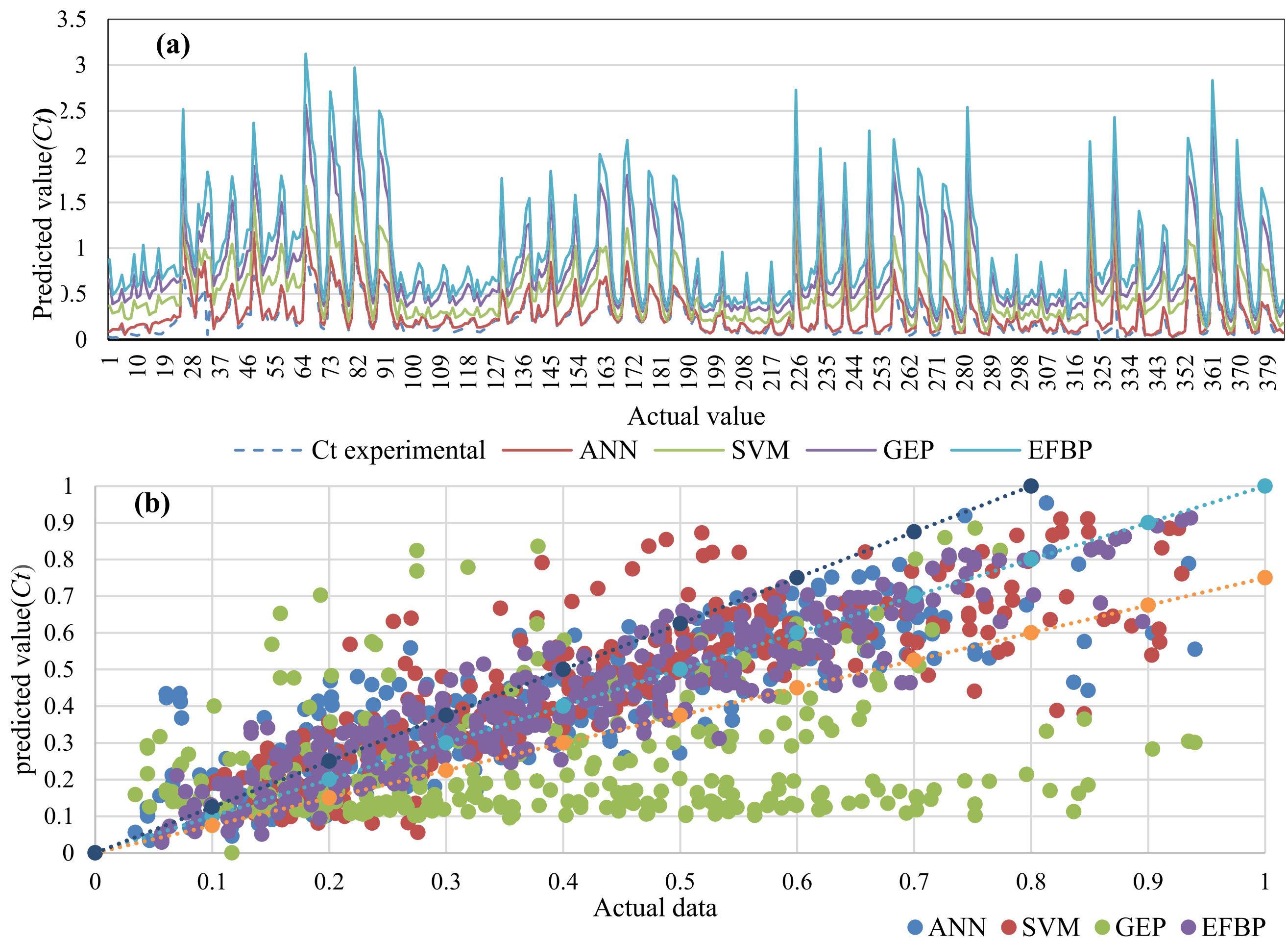

Fig. 9 (**a**) Line graphs of predicted vs. measured Ct and (**b**) Scatter plots by proposed methods.

Table 4 Descriptive statistics of the collected datasets (Ce)

Model	MSE	MAE	RMSE	R^2
ANN	0.01456	0.072985	0.1218476	0.93397
GEP	0.03479	0.1107729	0.18134	0.90
SVM	0.15647	0.12234	0.9865	0.96
EFBP	0.0266	0.16768	0.9356	0.95

wider scatter about the1:1 line. In contrast, the GEP model exhibited the weakest performance ($R^2 = 0.90$) with a wider scatter. Although the SVM showed a strong correlation ($R^2 = 0.96$), it also exhibited a higher prediction error (RMSE = 0.96), possibly due to overfitting at the extreme values. Despite these differences, the EFBP model shows reliable performance, especially in capturing the nonlinear behavior (*Ce*).

Figure 11a shows the line graphs comparing predicted and experimental (*Ce*) values. It is evident that ANN and SVM models effectively capture the sharp fluctuations at peak and trough points, indicating their adaptability to dynamic variations. While EFBP also follows the overall trend, its response around critical transitions is slightly less accurate than that of ANN. Conversely, the GEP model demonstrates limited tracking ability and shows a notable deviation compared the experimental values.

The scatter plots in Fig. 11b illustrates this difference. The ANN results are clustered closest to the 1:1 line, indicating the most accurate prediction, followed by the SVM and EFBP models. In contrast, the GEP shows a broader dispersion, suggesting less reliable predictions. Approximately 75% of ANN, SVM, and EFBP at a ± 25% error range, demonstrating strong predictive consistency. However, the wider point spread of EFBP indicates slightly higher uncertainty. ANN achieves the highest accuracy in predicting (*Ce*),

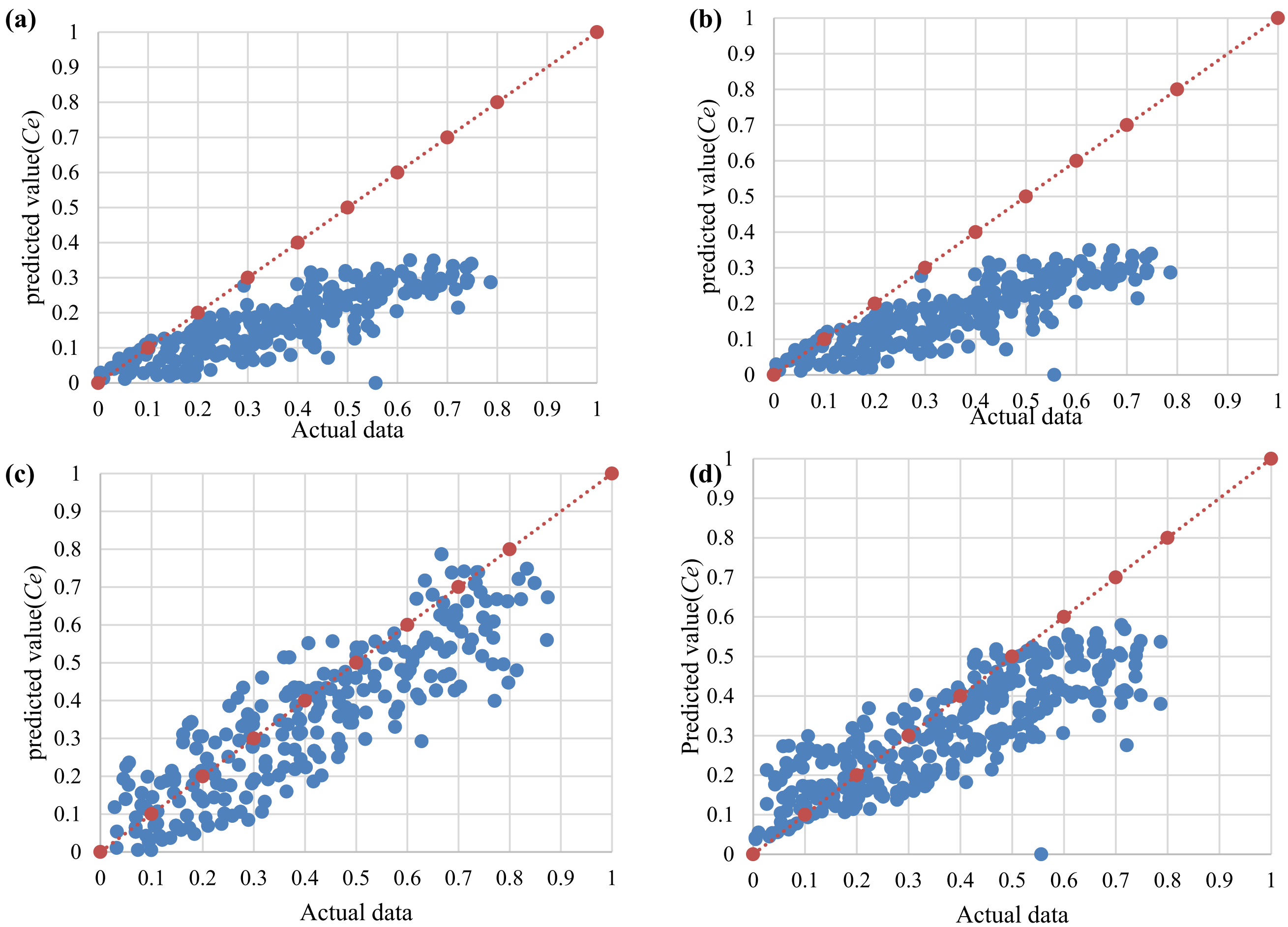

Fig. 10 Shows the comparison of the actual and the predicted **Ce** values using **a** ANN (**b**) GEP (**c**) SVM (**d**) EFBP models

and EFBP and SVM also achieve high accuracy, but GEP has less accuracy.

5.4 Sensitivity analysis

The sensitivity analysis presents data characteristics and facilitates the identification of the significance of the input parameters corresponding to the output. Figure 12 illustrates the importance of the input ratios (d/L, *B/L, Hi/L, d1/L, and d1/d2*) in predicting (*Cr, Ct*, and *Ce*(.

The result indicated that independent variables affected the dependent variables (*Cr* and *Ce*) by 11.11%, 22.22%, 22.22%, 11.11%, and 33.33%, respectively, while (*Ct*) was influenced by 28.75%, 21.48%, 14.29%, 5.66%, and 7.69%, respectively. The analysis revealed that relative depth (*d1/d2*), relative width (*B/L*), and wave steepness (*Hi/L*) have the most significant effects on (*Cr* (and (*Ce*(. In contrast, the relative depth (*d/L*) and relative draught (*d1/L*) have the least influence. Furthermore, the results demonstrate that (*Ct)* is primarily influenced by relative depth (*d/L*), relative width (*B/L*), and wave steepness (*Hi/L*).In contrast, relative draught (*d1/L*) and relative depth (*d/L*) have the least impact on the reflection coefficient.

6 Conclusions and future directions

This study developed and validated a novel Ensemble Floating Breakwater Prediction (EFBP) model to forecast the hydrodynamic performance of hybrid floating breakwater–Wave Energy Converter (WEC) systems. Experimental data were utilized to train the model and ensure its accuracy.

The shape of the floating breakwater plays a crucial role in wave energy conversion, with Model D demonstrating the optimal performance. The Enhanced Floating Breakwater Prediction (EFBP) model shows significant improvements in predictive accuracy compared to traditional models, achieving (R^2) of approximately 0.97, 0.96, and 0.95 for *Cr*, *Ct*, and *Ce*, respectively. These improvements enable optimized real-time power take-off (PTO) control and enhanced energy extraction efficiency, directly supporting design and operational strategies in wave energy-based coastal protection

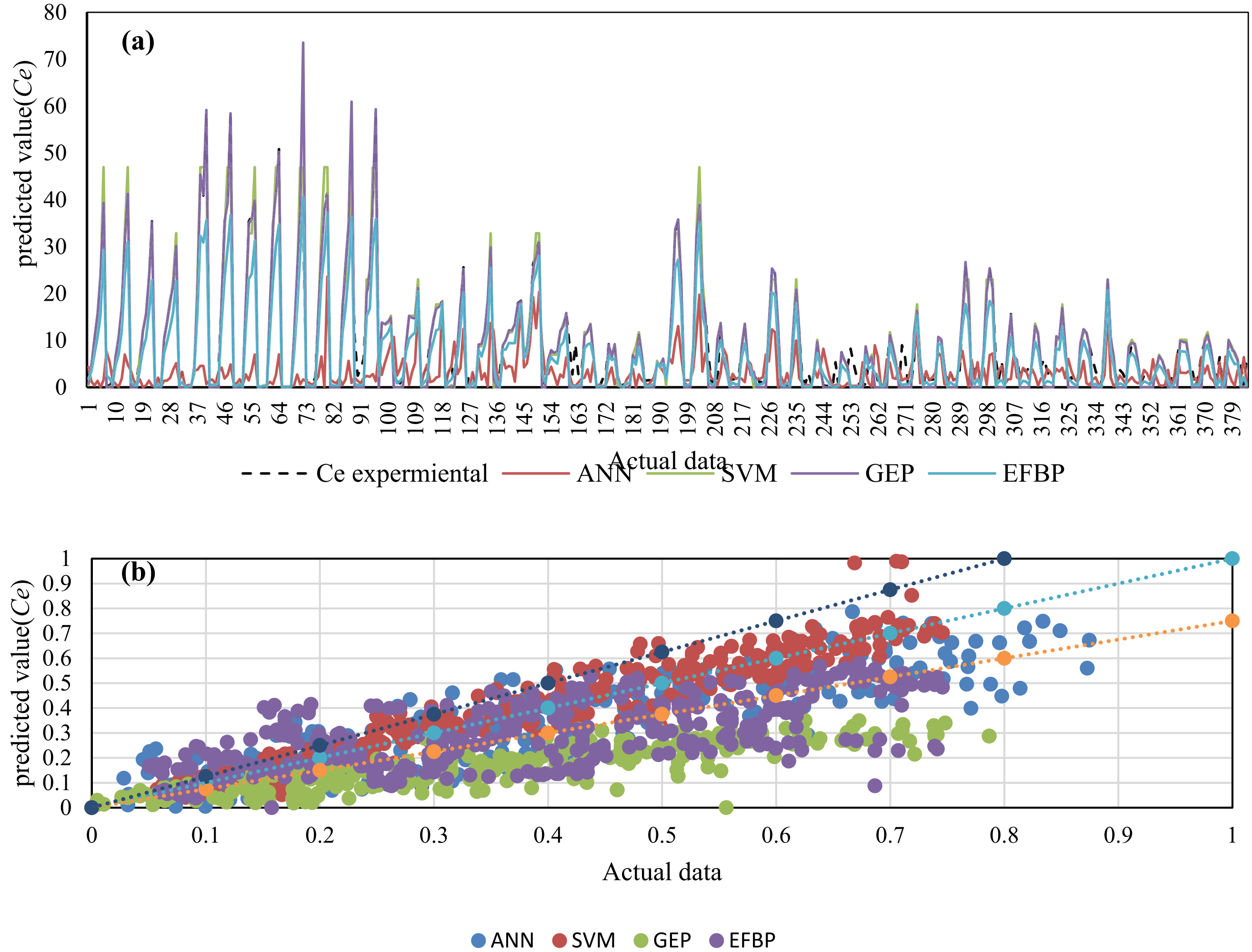

Fig. 11 (**a**) Line graphs of predicted vs. measured C**e** and (**b**) Scatter plots by proposed methods.

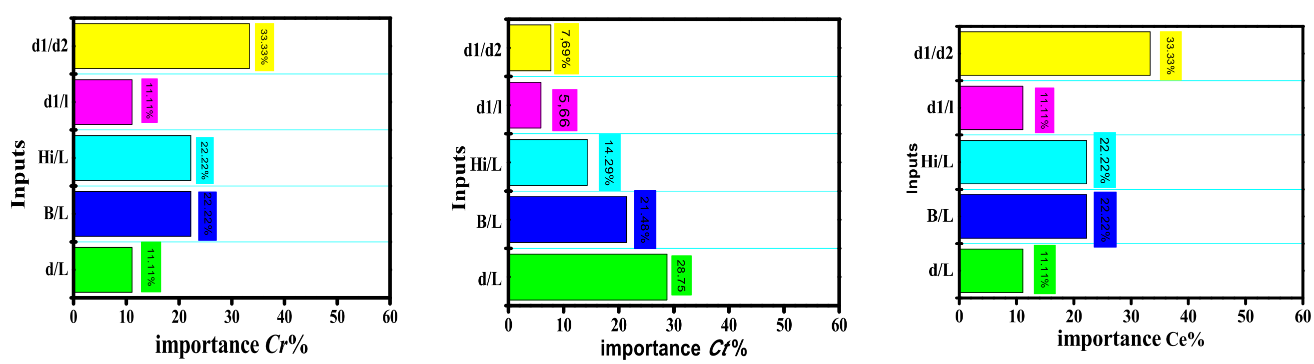

Fig. 12 Importance of the input ratios in predicting values

systems. Sensitivity analysis revealed that the relative depth (*d1/d2*) and wave steepness (*Hi/L*) have a notable effect on *Cr* and *Ce*, while the relative width (*B/L*) primarily influences *Ct*.

However, the 360 dataset is limited in scale and controlled conditions, which may not fully represent real-sea environments. Future validation using full-scale experiments or independent simulations, alongside expansion of datasets under diverse wave conditions, is essential to ensure robustness and practical applicability in offshore engineering.

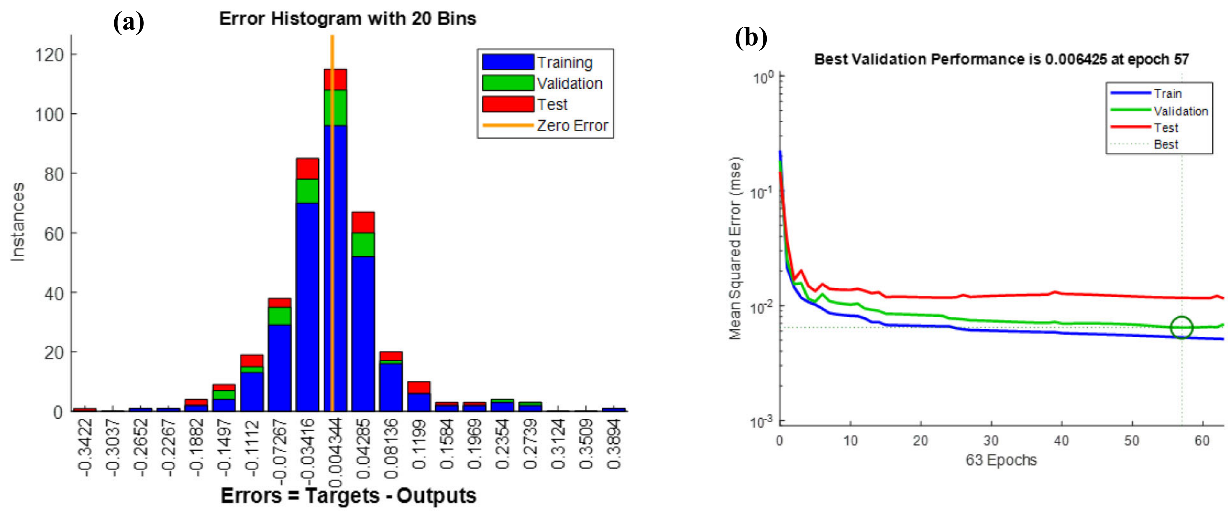

Fig. 13 ANN Model **a** Error Histogram **b** Validation Performance across Epochs

Appendix A. Additional technical details

A.1 Artificial neural network (ANN)

In this case, a single hidden-layer ANN was implemented, and the number of hidden nodes was selected using a trial-and-error approach. As illustrated in Fig. 13a, the best validation performance was achieved at epoch 30, corresponding to the minimum mean square error MSE value of 6.345e-03. This indicates a general trend of decreasing MSE with increasing epochs. Additionally, an error histogram was plotted in Fig. 13b to evaluate error density. As depicted, the error distribution is normal and more concentrated around zero. Based on the number of neurons in the hidden layer that resulted in the lowest MSE, the optimal ANN architecture was established as 5–10-1, as illustrated in Fig. 14a. In this architecture, the ANN model begins with an input layer containing five neurons, each representing one of the input ratios. This is followed by a hidden layer of 10 neurons that use the sigmoid activation function to process the data. Figure 14b shows the ANN model prediction of the floating breakwater's *Cr*, *Ct*, and *Ce* coefficients using five ratios (*d/L*, *Hi/L*, *B/L*, *d1/d*, *d1/d2*) as inputs.

Equation (11) was developed based on the ANN model for predicting the output coefficients. It can be expressed as follows:

$$Output = \frac{\left[\mathrm{W2}\left\{\frac{2}{1+\exp[-2(\mathrm{W1X+B1})]]}\right\}\right] + \mathrm{B2} + 1}{7.692} + 0.32 \tag{11}$$

where X is the input layer matrix, B1 is the vector of weights of the bias neurons in the hidden layer, *B2* is the vector of weights of the bias neurons in the output layer, W1 is the connection weight matrix between the neurons of the input and hidden layer, and W2 is the connection weight matrix between the hidden and output layers. In the context of the described ANN model, the vectors of *X,* B1, B2, W1, and W2 can be represented as follows:

$$X = \begin{bmatrix} 2.12\left(\frac{\mathrm{d}}{\mathrm{L}} - 0.1598\right) - 1 \\ 14.21\left(\frac{\mathrm{hi}}{\mathrm{L}} - 0.0121\right) - 1 \\ 2.312\left(\frac{\mathrm{B}}{\mathrm{L}} - 0.1896\right) - 1 \\ 6.31\left(\frac{\mathrm{dr1}}{\mathrm{d}} - 0.133\right) - 1 \\ 2.129\left(\frac{\mathrm{d1}}{\mathrm{d}} - 0.060\right) - 1 \end{bmatrix}$$

$$; B1 = \begin{bmatrix} -3.0978 \\ -5.110 \\ 2.956 \\ 0.9739 \\ -1.684 \\ 0.904 \\ 3.564 \\ 1.615 \\ 2.982 \\ 4.362 \end{bmatrix}$$

$$; B2 = [0.5664] \tag{12}$$

W1 = [arrayccccc10.427 -0.006 -0.972 0.787 -3.25 -0.366 0.107 -3.26 -3.52 0.239 0.151 3.71 0.155 -1.96 -0.193 1.80 1.37 0.470 2.18 -0.376 1.38 0.091 -0.152 0.680 -3.14 -0.304 0.219 0.955 0.251 -2.57 0.229 -4.31 0.005 2.91 0.135 0.662 0.0452 0.552 -0.351 1.73 -2.30 2.64 2.34 -0.066 -0.0137 1.30 -0.166 4.6 2.7 -0.229].

W2 = [-2.13 -1.11 0.914 -0.123 2.33 -2.29 0.83 -2.08 -0.493 -1.38].

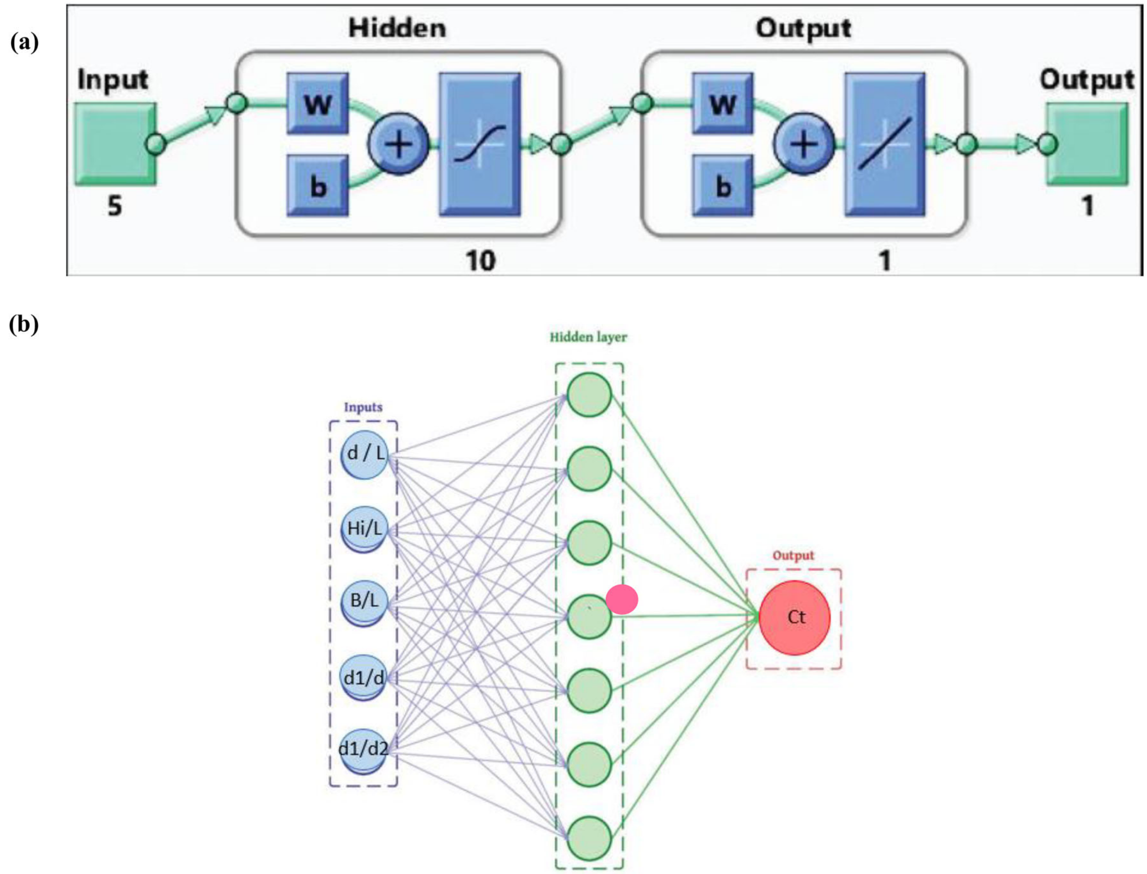

Fig. 14 The architecture of artificial neural network **a** Schematic diagram of the developed ANN model by the MATLAB software **b** Inputs and output of the ANN model

Table 5 Applied setting for developed models

Method	Category	Parameters	Values
GEP	General settings	Quantity of chromosomes	30
	Fitness	Quantity of genes	3
	Quantitative Constants	Head size	8
		Tail size	25
		Gene size	58
		Linking function	Multiplication
		Function	RMSE (Root Mean Square Error)
		Data type	Floating-point
ANN	General settings	epoch	30
		Hidden layer	10
		Function	linear activation

A.2 Gene expression programming (GEP)

After conducting multiple experiments, it was observed that the fitness function values and the coefficient of determination for both training and testing datasets remained nearly unchanged after 219,016 generations, suggesting that the number of generations may cease. To create the best model of the GEP, which takes the form of an algebraic equation between the input and output variables, all mentioned parameters were selected using the trial-and-error technique. Table 5 shows general settings for the developed models.

Equation (13) was derived from the GEP model to predict the output coefficient and is presented as follows:

$$y = \frac{1}{2}\left[1.0 - \left(\frac{d_2}{d} + \frac{B}{L} + \frac{2H_i}{L}\right)^2 + \frac{B}{L}\right]^2$$

$$+\tanh\left(\tanh\left[\left(3.692\cdot\frac{d}{L}\cdot\tanh\left(\frac{d}{d}\right)\right)+\left(\frac{B}{L}+\frac{d}{L}/2\right)^2\right]\right)$$
$$+\left(1.0-\left(1.0-\left(1.0-\frac{d}{L}\right)\cdot\left(5.37-\frac{H_i}{L}\right)\right)\right)$$
$$-gepMax2\left(gep3Rc\left(\frac{H_i}{L},\frac{B}{L}\right)\right)\right) \quad (13)$$

Acknowledgements The authors would like to thank the Faculty of Engineering, Port Said University, Port Said, Egypt, for its support.

Author contributions Bayan Hamed performed the experiments, analyzed the results, and wrote the original draft. Mohamed Elkiki was the main supervisor of the research, reviewed the written work, and supervised the experiments. Sherif Abd-ella contributed to review and editing. Asmaa H. Rabie and Reda Diab played the main role in the technical review and presentation of the manuscript. All authors reviewed and approved the final manuscript.

Funding Open access funding provided by The Science, Technology & Innovation Funding Authority (STDF) in cooperatsion with The Egyptian Knowledge Bank (EKB).

Data availability No datasets were generated or analysed during the current study.

Declarations

Conflict of interests The authors declare no competing interests.

Open access This article is licensed under a Creative Commons Attribution 4.0 International License, which permits use, sharing, adaptation, distribution, and reproduction in any medium or format, as long as you give appropriate credit to the original author(s) and the source, provide a link to the Creative Commons license, and indicate if changes were made. The images or other third-party material in this article are included in the article's Creative Commons license, unless indicated otherwise in a credit line to the material. If material is not included in the article's Creative Commons license and your intended use is not permitted by statutory regulation or exceeds the permitted use, you will need to obtain permission directly from the copyright holder. To view a copy of this license, visit http://creativecommons.org/licenses/by/4.0/.

Open Access This article is licensed under a Creative Commons Attribution 4.0 International License, which permits use, sharing, adaptation, distribution and reproduction in any medium or format, as long as you give appropriate credit to the original author(s) and the source, provide a link to the Creative Commons licence, and indicate if changes were made. The images or other third party material in this article are included in the article's Creative Commons licence, unless indicated otherwise in a credit line to the material. If material is not included in the article's Creative Commons licence and your intended use is not permitted by statutory regulation or exceeds the permitted use, you will need to obtain permission directly from the copyright holder. To view a copy of this licence, visit http://creativecommons.org/licenses/by/4.0/.

References

Abdi Chooplou C, Kahrizi E, Fathi A, Ghodsian M, Latifi M (2024) Baffle-enhanced scour mitigation in rectangular and trapezoidal piano key weirs: An experimental and machine learning Investigation. Water 16(15):2133. https://doi.org/10.3390/w16152133

Alshahri AH, Elbisy MS (2023) Assessment of using artificial neural network and support vector machine techniques for predicting wave-overtopping discharges at coastal structures. J Mar Sci Eng 11(3):539. https://doi.org/10.3390/jmse11030539

Ashlin SJ, Sundar V, Sannasiraj SA (2016) Effects of bottom profile of an oscillating water column device on its hydrodynamic characteristics. Renew Energy 96:341–353. https://doi.org/10.1016/j.renene.2016.04.091

Azamathulla HM (2012) Gene expression programming for prediction of scour depth downstream of sills. J Hydrol 460:156–159. https://doi.org/10.1016/j.jhydrol.2012.06.034

Balas CE, Koç ML, Tür R (2010) Artificial neural networks based on principal component analysis, fuzzy systems and fuzzy neural networks for preliminary design of rubble mound breakwaters. Appl Ocean Res 32(4):425–433. https://doi.org/10.1016/j.apor.2010.09.005

Bishop CT (1982) Floating tire breakwater design comparison. J Waterway Port Coast Ocean Div 108(3):421–426

Bungay PDS (2021) 'Proposal for a new graduate program: Master of Artificial Intelligence'.

Castro A, Carballo R, Iglesias G, Rabuñal JR (2014) Performance of artificial neural networks in nearshore wave power prediction Appl Soft. Comput J 23(194):201. https://doi.org/10.1016/j.asoc.2014.06.031

Çelik A (2022) An experimental investigation into the effects of front wall geometry on OWC performance for various levels of applied power take off dampings. Ocean Eng 248:110761. https://doi.org/10.1016/j.oceaneng.2022.110761

Clauss G, Lehmann E, Östergaard C (1992) Hydromechanical analysis of offshore structures. Offshore Structures: Volume I: Conceptual Design and Hydromechanics. Springer, pp 145–332

Cogdill RP, Dardenne P (2004) Least-squares support vector machines for chemometrics: an introduction and evaluation. J near Infrared Spectrosc 12(2):93–100

Dalinghaus C, Coco G, Higuera P (2022) A predictive equation for wave setup through the use of genetic programming. Coast Eng Proc 37:15. https://doi.org/10.9753/icce.v37.waves.15

Deng L, Hinton G, Kingsbury B (2013) 'New types of deep neural network learning for speech recognition and related applications: An overview', in *2013 IEEE international conference on acoustics, speech and signal processing*. IEEE, pp. 8599–8603. https://doi.org/10.1109/ICASSP.2013.6639344.

Deo MC, Jagdale SS (2003) Prediction of breaking waves with neural networks. Ocean Eng 30(9):1163–1178. https://doi.org/10.1016/S0029-8018(02)00086-0

Deo MC, Jha A, Chaphekar AS, Ravikant K (2001) Neural networks for wave forecasting. Ocean Eng 28(7):889–898. https://doi.org/10.1016/S0029-8018(00)00027-5

Elbisy MS (2015) Sea wave parameters prediction by support vector machine using a genetic algorithm. J Coast Res 31(4):892–899. https://doi.org/10.2112/JCOASTRES-D-13-00087.1

Elhanafi A, Fleming A, Macfarlane G, Leong Z (2017) Underwater geometrical impact on the hydrodynamic performance of an offshore oscillating water column–wave energy converter'. Renew Energy 105:209–231. https://doi.org/10.1016/j.renene.2016.12.039

Eltarabily MG, Elshaarawy MK, Elkiki M, Selim T (2024) Computational fluid dynamics and artificial neural networks for modelling lined irrigation canals with low-density polyethylene and cement concrete liners. Irrigat Drain 73(3):910–927. https://doi.org/10.1002/ird.291

Fan Z, Yan Z, Wen S (2023) 'Deep learning and artificial intelligence in sustainability: a review of SDGs, renewable energy, and environmental health. Sustainability 15(18):13493

Ferreira, C. (2010) 'What is gep? from genexprotools tutorials-a gepsoft web resource'.
Formentin SM, Zanuttigh B, Van Der Meer JW (2017) A neural network tool for predicting wave reflection, overtopping and transmission. Coast Eng J. https://doi.org/10.1142/S0578563417500061
Garrido JM, Medina JR (2012) New neural network-derived empirical formulas for estimating wave reflection on Jarlan-type breakwaters. Coast Eng 62:9–18. https://doi.org/10.1016/j.coastaleng.2011.12.003
Ghasemi H, Kolahdoozan M, Pena E, Ferreras J, Figuero A (2016) A new hybrid ANN model for evaluating the efficiency of Î-Type floating breakwater. Coast Eng Proc 35:25. https://doi.org/10.9753/icce.v35.structures.25
Gupta A, Karmakar D (2023) 'Prediction of Hydrodynamic Performance of Submerged Composite Porous Breakwater Using Support Vector Machine', in *International Conference on Communication and Computational Technologies*. Springer, pp. 137–148.
Guven A, Gunal M (2008) Genetic programming approach for prediction of local scour downstream of hydraulic structures. J Irrig Drain Eng 134(2):241–249. https://doi.org/10.1061/(ASCE)0733-9437(2008)134:2(241)
Han D, Chan L, Zhu N (2007) Flood forecasting using support vector machines. J Hydroinformatics 9(4):267–276. https://doi.org/10.2166/hydro.2007.027
Harikrishnan GR, Sreedharan S (2025) Advanced short-term load forecasting for residential demand response: an XGBoost-ANN ensemble approach. Electr Power Syst Res 242:111476. https://doi.org/10.1016/j.epsr.2025.111476
Harms VW (1979) Design criteria for floating tire breakwaters. J Waterway Port Coast Ocean Div 105(2):149–170
Hashmi MZ, Shamseldin AY, Melville BW (2011) Statistical downscaling of watershed precipitation using gene expression programming (GEP). Environ Model Softw 26(12):1639–1646. https://doi.org/10.1016/j.envsoft.2011.07.007
Howe D, Nader J-R, Macfarlane G (2020) Experimental investigation of multiple oscillating water column wave energy converters integrated in a floating breakwater: energy extraction performance. Appl Ocean Res 97:102086. https://doi.org/10.1016/j.apor.2020.102086
Jalani MA, Ismail NI, Saad MR, Samion MK, Imai Y, Nagata S, Rahman MR (2022) Experimental study on a bottom corner of the floating WEC. Ocean Eng 243:110237. https://doi.org/10.1016/j.oceaneng.2021.110237
Jeng D-S, Cha DF, Blumenstein M (2004) Neural network model for the prediction of wave-induced liquefaction potential. Ocean Eng 31(17–18):2073–2086. https://doi.org/10.1016/j.oceaneng.2004.05.006
Karami H, Saghi H (2024) Hybrid intelligent and numerical methods to estimate the transmission coefficients of rectangular floating breakwaters. Water Supply 24(9):3015–3030. https://doi.org/10.2166/ws.2024.175
Kennedy RJ, Marsalek J (1969) Flexible porous floating breakwaters. Coast Eng 1968:1095–1103
Kim DH, Kim YJ, Hur DS (2014) Artificial neural network based breakwater damage estimation considering tidal level variation. Ocean Eng 87:185–190. https://doi.org/10.1016/j.oceaneng.2014.06.001
Kim T, Kwon S, Kwon Y (2021) Prediction of wave transmission characteristics of low-crested structures with comprehensive analysis of machine learning. Sensors. https://doi.org/10.3390/s21248192
Kuntoji G, Rao M, Rao S (2020) Prediction of wave transmission over submerged reef of tandem breakwater using PSO-SVM and PSO-ANN techniques. ISH J Hydraul Eng 26(3):283–290. https://doi.org/10.1080/09715010.2018.1482796
Lee TL, Tsai CP, Lin HM, Fang CJ (2009) A combined thermographic analysis—Neural network methodology for eroded caves in a seawall. Ocean Eng 36(15–16):1251–1257. https://doi.org/10.1016/j.oceaneng.2009.07.009
López I, Carballo R, Fouz DM, Iglesias G (2021) Design selection and geometry in OWC wave energy converters for performance. Energies 14(6):1707. https://doi.org/10.3390/en14061707
Loukili M, El Moumni S, Kotrasova K (2025) AI-driven optimization of breakwater design: predicting wave reflection and structural dimensions. Fluids 10(2):34. https://doi.org/10.3390/fluids10020034
Mahjoobi J, Mosabbeb EA (2009) Prediction of significant wave height using regressive support vector machines. Ocean Eng 36(5):339–347. https://doi.org/10.1016/j.oceaneng.2009.01.001
Malara G, Gomes RP, Arena F, Henriques JC, Gato LM, Falcão AF (2017) The influence of three-dimensional effects on the performance of U-type oscillating water column wave energy harvesters. Renew Energy 111:506–522. https://doi.org/10.1016/j.renene.2017.04.038
Mandal S, Rao S, Raju DH (2005) Ocean wave parameters estimation using backpropagation neural networks. Mar Struct 18(3):301–318. https://doi.org/10.1016/j.marstruc.2005.09.002
Nawaz U, Anees-ur-Rahaman M, Saeed Z (2025) A survey of deep learning approaches for the monitoring and classification of seagrass. Ocean Sci J 60(2):19. https://doi.org/10.1007/s12601-025-00213-1
Oliver JM, Esteban MD, López-Gutiérrez JS, Negro V, Neves MG (2021) Optimizing wave overtopping energy converters by ANN modelling: Evaluating the overtopping rate forecasting as the first step. Sustainability 13(3):1483. https://doi.org/10.3390/su13031483
Patil SG, Mandal S, Hegde AV, Alavandar S (2011) Neuro-fuzzy based approach for wave transmission prediction of horizontally interlaced multilayer moored floating pipe breakwater'. Ocean Eng 38(1):186–196. https://doi.org/10.1016/j.oceaneng.2010.10.009
Peng, W. et al. (2024) Effect of varying PTO on a triple floater wave energy converter-breakwater hybrid system: an experimental study, Renewable Energy, 224:120100.
Patil SG, Mandal S, Hegde AV (2012) Genetic algorithm based support vector machine regression in predicting wave transmission of horizontally interlaced multi-layer moored floating pipe breakwater. Adv Eng Softw 45(1):203–212. https://doi.org/10.1016/j.oceaneng.2010.10.009
Portillo JN, Rodríguez JO, del Campo JM, Valdecantos VN (2024) Artificial intelligence in coastal engineering: application to climate change studies. J Coast Res 113:180–184. https://doi.org/10.2112/JCR-SI113-036.1
Ram G, Saad MR, Abidin NZ, Rahman MR (2022) Hydrodynamic performance of a hybrid system of a floating oscillating water column and a breakwater. Ocean Eng 264:112463. https://doi.org/10.1016/j.oceaneng.2022.112463
Robertson B, Gharabaghi B, Power HE (2017) Predicting breaking wave conditions using gene expression programming. Coast Eng J 59(03):1750017. https://doi.org/10.1142/S0578563417500176
Samui P, Dixon B (2012) Application of support vector machine and relevance vector machine to determine evaporative losses in reservoirs. Hydrol Process 26(9):1361–1369. https://doi.org/10.1002/hyp.8278
Seif Y, Arman A, Rahmanshahi M (2024) Multi-approach assessment for predicting submerged discharge reduction factor in porous broad-crested weirs (Preprint). Research Square. https://doi.org/10.21203/rs.3.rs-4110223/v1.
Shirlal KG, Rao S (2008) Performance of a submerged reef–a physical model study. Int J Ecol Develop 11:90–99
Suykens JAK, Vandewalle J (1999) Least squares support vector machine classifiers. Neural Process Lett 9(3):293–300

Teh HM, Ismail H (2013) 'Hydraulic characteristics of a stepped-slope floating breakwater', in *IOP Conference Series: Earth and Environmental Science*. IOP publishing, p. 12060.

Tseng CM, Jan CD, Wang JS, Wang CM (2007) Application of artificial neural networks in typhoon surge forecasting. Ocean Eng 34(11–12):1757–1768. https://doi.org/10.1016/j.oceaneng.2006.09.005

Van Gestel T, Suykens JA, Baesens B, Viaene S, Vanthienen J, Dedene G, De Moor B, Vandewalle J (2004) Benchmarking least squares support vector machine classifiers. Mach Learn 54(1):5–32

Zanuttigh B, Formentin SM, Briganti R (2013) A neural network for the prediction of wave reflection from coastal and harbor structures. Coast Eng 80:49–67. https://doi.org/10.1016/j.coastaleng.2013.05.004

Zhang X, Ma S, Duan W (2018) A new L type floating breakwater derived from vortex dissipation simulation. Ocean Eng 164:455–464. https://doi.org/10.1016/j.oceaneng.2018.06.059

Publisher's Note Springer Nature remains neutral with regard to jurisdictional claims in published maps and institutional affiliations.